Supporting Information for:

Distribution Depth of Stone Consolidants Applied On-Site: Analytical Modelling with Field and Lab Cross-Validation

Matea Ban [a,2,*], Laura Aliotta [b,2], Vito Gigante [b,2], Elisabeth Mascha [c], Antonella Sola [d,1] and Andrea Lazzeri [b]

[a] Institute of Geotechnics, Faculty of Civil Engineering, TU Wien, Austria

[b] Department of Civil and Industrial Engineering, University of Pisa, Italy; laura.aliotta@dici.unipi.it, vito.gigante@dici.unipi.it and andrea.lazzeri@unipi.it

[c] Institute of Art and Technology, Conservation Science, University of Applied Arts Vienna, Austria; elisabeth.mascha@uni-ak.ac.at

[d] Department of Engineering 'Enzo Ferrari', University of Modena and Reggio Emilia, Italy; antonella.sola@unimore.it

* Corresponding author: matea.ban@tuwien.ac.at

[1] Present address: Commonwealth Scientific and Industrial Research Organisation, Manufacturing Business Unit, Metal Industries Program, Clayton, VIC, Australia; antonella.sola@csiro.au

[2] These authors contributed equally to the work

CONTENTS

Table S1. Petrographic description of the studied lithotype *St. Margarethen*.

General description		
Provenience	St. Margarethen (Burgenland, Leithagebirge, Austria). The so-called "Roman quarry" of St. Margarethen in Burgenland was an important Leithakalk quarry in eastern Austria with an exploitation history dating back to the roman times. The characteristic detritic limestone has been used since as dimension stone for buildings, monuments and their restoration. [1]	
Commercial name	*St. Margarethen* Leithakalk	
Petrographic Group	Sedimentary rock	
Petrographic Family	Biogeneous sedimentary rock	
Lithotype	Biosparite, grainstone, calcareous arenite	
Typical color	Yellowish-brown to light grey	
Geological age	Miocene/Langhian-Serravallian: Badenian	
Petrographic description		
Components	Composed mainly of small fragments of coralline algae and foraminifera. Additionally, echinoderms, fragments of serpulides and ostracods can be observed.	
Granulometry and texture	In thin sections it occurs very porous and is composed mainly of small fragments of coralline red algae and foraminifera.	
Grain contacts and binder minerals	Components are cemented with microsparitic calcite, a fine-grained calcite.	
Technical Data [2]		
Stone properties	**Homogenous variety**	**Coarse-grained variety**
Bulk density	2030 kg/m³	2060 kg/m³
Open porosity	15.2 Vol. %	11.2 Vol. %
Water absorption	7.5 M.%	5.4 M.%
Sound speed propagation	3.37-3.52 km/s	3.55 - 4.20 km/s
Compressive strength	25.4 (19.3 - 30.9) N/mm^2	---
Bending tensile strength	5.25 (3.03 - 8.08) N/mm^2	---

See **Figure S1** for details on components, granulometry and texture as well as the binder material.

The preparation of samples is done by vacuum-embedding of the specimen in a blue dyed epoxy resin (Araldite® 2020). Blue colored epoxy resin is used in order to improve the visualization of the open pore spaces. Petrographic thin sections of about 25 µm thickness as well as polished cross sections were produced perpendicular to the surface.

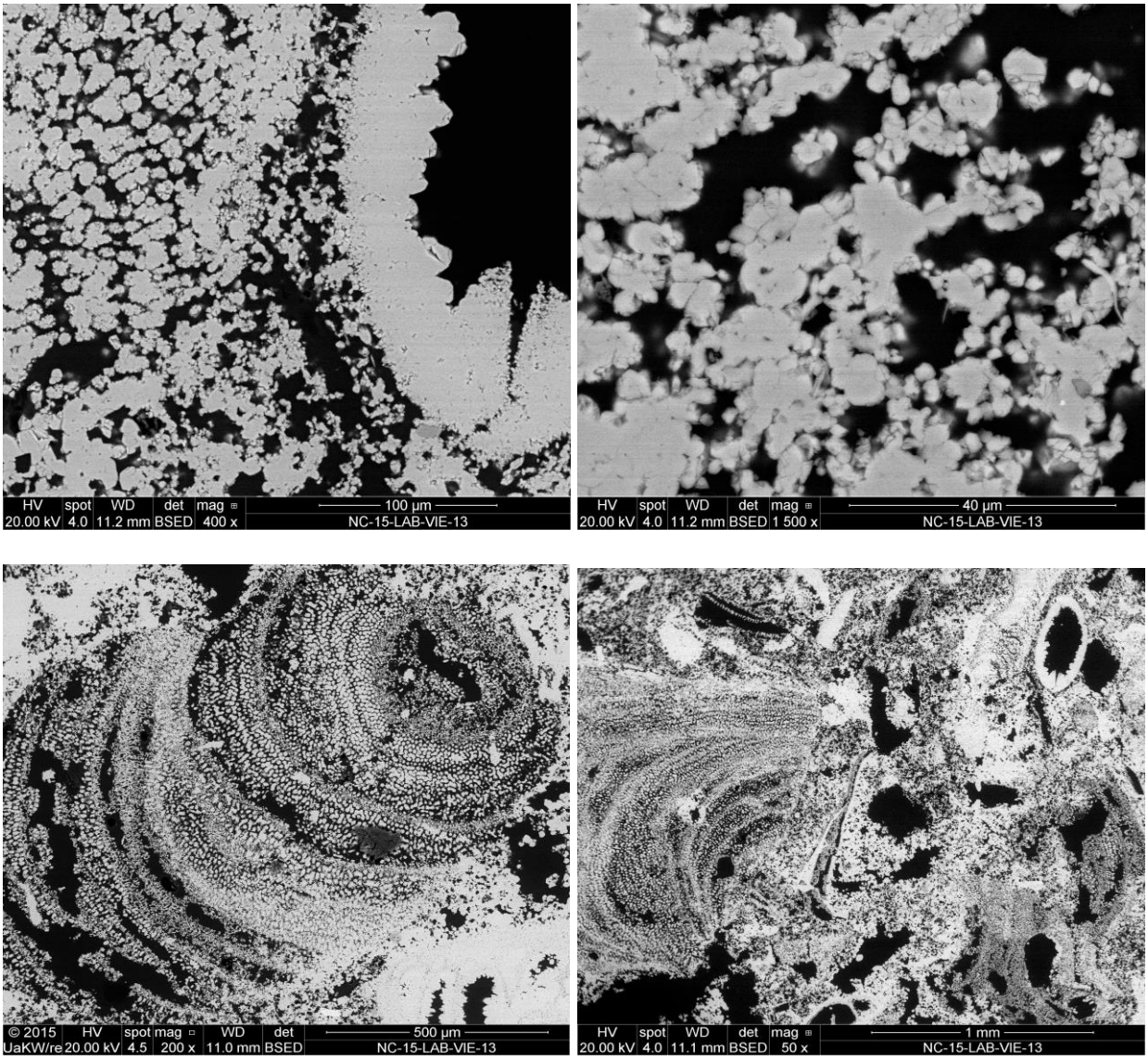

Figure S1. Details of the microstructure exhibiting the rich textural and structural diversity of *St. Margarethen.* Figures at the top show details of the cementation, with the fine-grained calcite, while the bottom figures exhibit fragments of foraminifera (*Heterostegina sp.*).

Table S2. Porometric data from mercury intrusion tests for *St. Margarethen* specimens in fresh conditions with corresponding total pore size.

Characteristics	**Double determination**		**Pore diameter ranges [µm]**	**Porosity 1st test [%]**	**Porosity 2nd test [%]**
Number of tests	1st test	2nd test	150-125	0.000	0.000
Total pore surface [m^2/g]	0.82	3.08	125-100	1.373	2.920
Average pore diameter [µm]	0.48	0.14	100-50	7.184	7.621
Hg-total porosity [%]	20.65	22.54	50-20	4.070	3.925
			20-10	1.661	1.530
			10-5	1.209	1.106
			5-2	1.281	1.061
			2-1	0.865	0.748
			1-0.5	0.710	0.676
			0.5-0.2	0.656	0.546
			0.2-0.1	0.407	0.313
			0.1-0.05	0.386	0.507
			0.05-0.02	0.807	0.166
			0.02-0.01	0.037	0.750
			0.01-0.005	0.000	0.656
			0.005-0.002	0.000	0.000
			0.002-0.001	0.000	0.000

Note that the difference between the determined values (e.g. total pore surface) can be attributed to the intrinsic properties of this lithotype, that is, its textural and structural inhomogeneity. Moreover, mercury intrusion porosimetry tests use rather small specimens (1 cm^3), exaggerating the effect of aggregate size and are therefore prone to deliver less meaningful results for such lithotypes in fresh or weathered conditions.

Determination of Frost Resistance after EN 12371

The effect of freeze/thaw cycles on *St. Margarethen* was studied according to the Test B recommended in the EN 12371 standard. The test allows for estimating the mass loss after 168 freeze/thaw cycles; moreover, in order to quantify the effects of freeze/thaw cycles on the petro-physical proprieties of the stones, ultrasound velocity and Young's modulus have been measured before testing and after 14, 56, 84, 140 and 168 cycles.

The test has been carried out on six specimens. A total of 168 freeze/thaw cycles have been carried out. Each cycle consists of a 6 h freezing period in air (temperature variation from +20 °C to –12 °C within the 6h), followed by a 6 h thawing period (+5 °C < T < 20 °C) during which the specimens are immersed in water. At the end of the tests (168 cycles), specimens have been weighted to estimate the possible loss of weight; finally, ultrasound velocity and Young's modulus have been measured. Before the testing and after the 168 cycles the change in apparent volume according to EN 1936 was measured. Afterwards the specimens have been left under water for 48h.

For all testing's the specimens were dried at 70 °C until a constant mass was reached. For determination of ultrasound pulse velocity and the Young's modulus the device from *Geotron-Elektronik* was used (see the corresponding manuscript for the details on the device). The climatic chamber MA-C314 with a controller MA-C314ET acquired from Austro Test Hrdina GmbH came to use.

Table S3. Loss of weight [wt-%] after 168 freeze-thaw cycles.

SM_0	SM_{168}	[Δg]	[Δwt-%]
1378.30	1376.20	2.10	0.152
1754.91	1753.20	1.71	0.097
1425.98	1422.90	3.08	0.216

Table S4. Change of compressional wave velocities Vp [km/s] after 168 freeze-thaw cycles.

SM_0	SM_{168}	ΔV_p	ΔV_p [%]
3.57	3.22	0.34	9.67
5.22	4.93	0.29	5.50
3.86	3.69	0.17	4.44

Table S5. Change of Young's modulus [kN/mm^2] after 168 freeze-thaw cycles.

SM_0	SM_{168}	ΔE_d	ΔE_d [%]
21.480	10.285	11.195	52
50.977	49.140	1.837	4
23.492	23.119	0.373	2

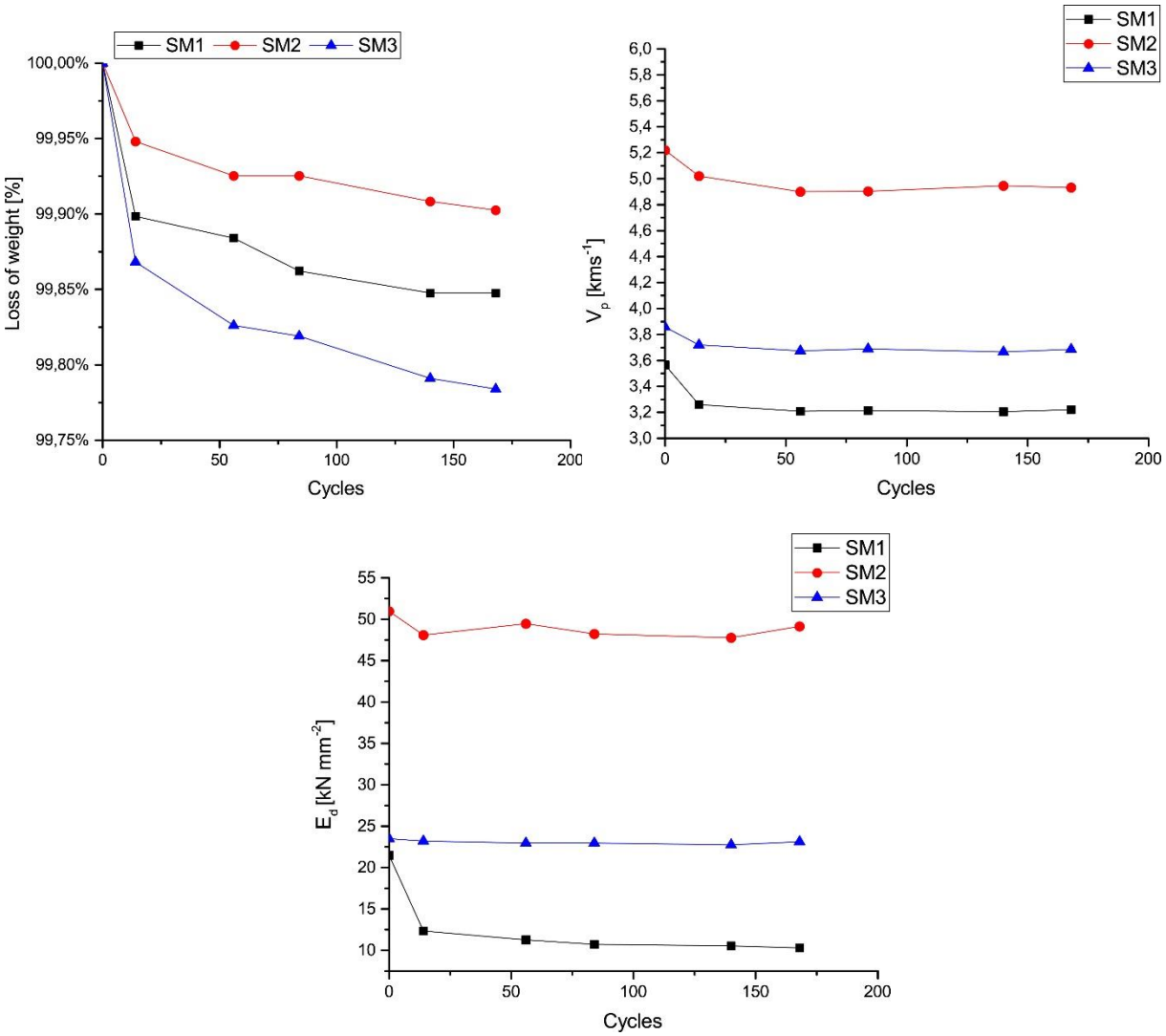

Figure S10. Corresponding visualization for Table S3 to S5

Table S6. Change in apparent volume

Sample	Apparent Vol. V_{b0} [ml] before and after 168 cycles	Note
SM1	730 to 725	
SM2	744 to 739	
SM3	732 to 723	
SM4	---	Specimens with major cracks and/or broken (e.g. **Fig. S2**)
SM5	---	
SM6	---	

Table S7. Visual inspection

Sample / Cycles	14	56	84	140	168
SM1	4	---	---	---	---
SM2	0	0	0	1	1
SM3	0	4	---	---	---
SM4	4	---	---	---	---
SM5	0	0	4	---	---
SM6	0	0	0	1	1

After the freeze-thaw cycles, the specimens are examined on all faces and sides and their behaviour is scored using the following scale:(**0)** specimen intact. (**1)** very minor damage (minor rounding of corners and edges) which does not compromise the integrity of the specimen. (**2)** one or several minor cracks (≤ 0,1 mm width) or detachment of small fragments (≤ 30 mm^2 per fragment). (**3)** one or several cracks, holes or detachment of fragments larger than those defined for the '2' rating, or alteration of material in veins, or the specimen shows important signs of crumble or dissolution. And, (**4)** specimen with major cracks or broken in two or more or disintegrated. The number of cycles at which the score of the visual examination attains 3 is noted.

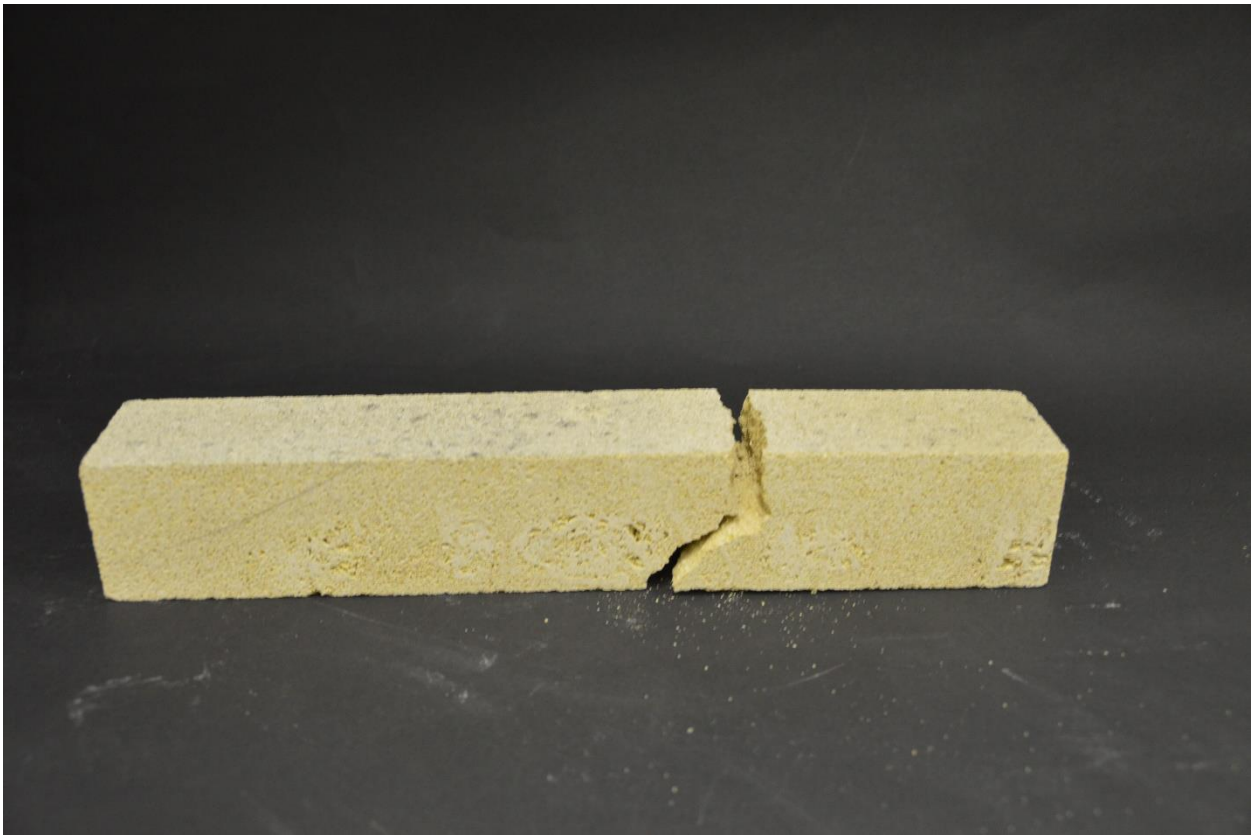

Figure S2. *St. Margarethen* after 56 cycles. Complete failure of the sample.

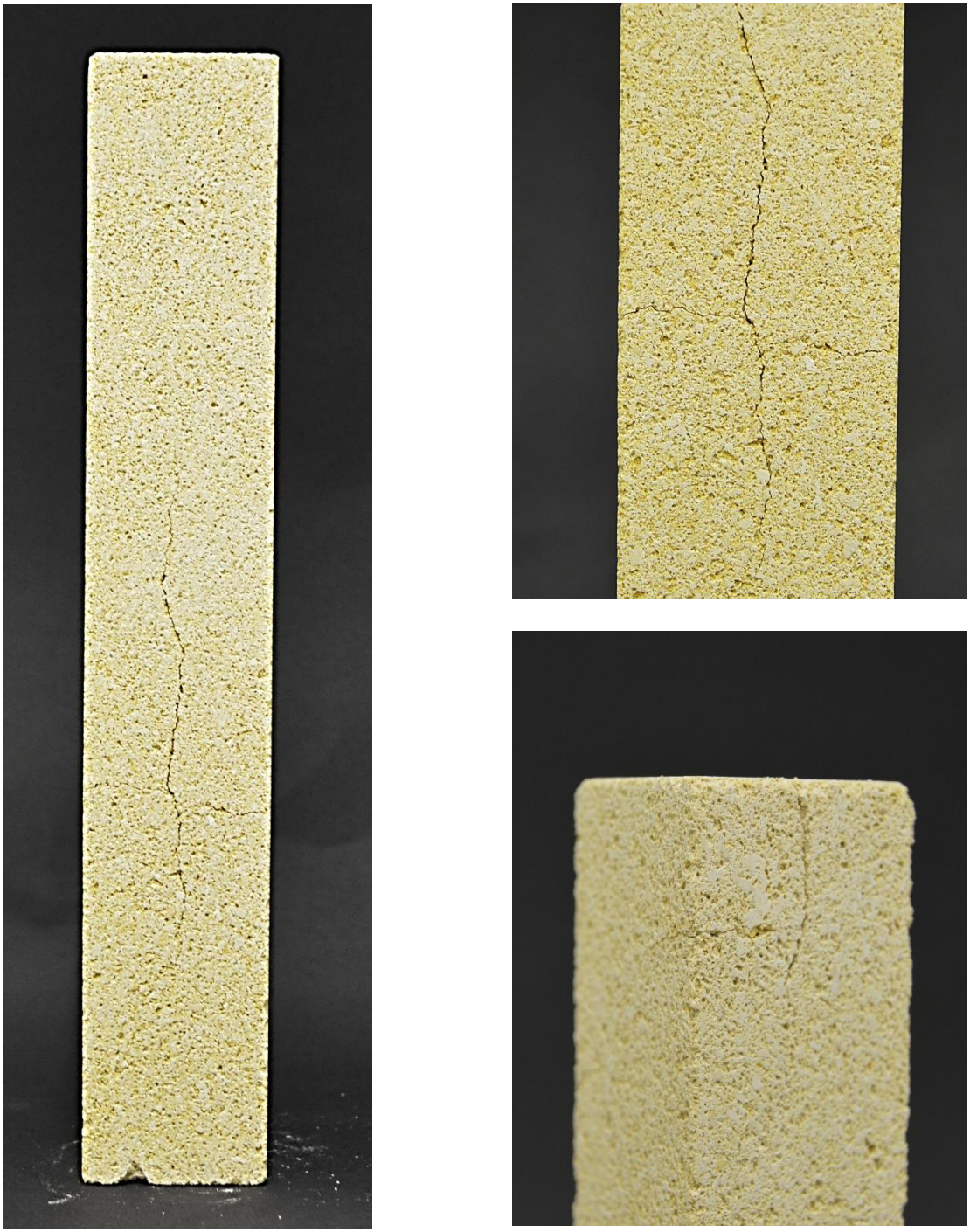

Figure S3. *St. Margarethen* after 14 cycles. Occurance of major cracks.

Interpretation and evaluation

Different intrinsic and extrinsic properties (*e.g.* porosity, temperature, presence of salt and humidity, etc.) influence the frost-thaw resistance of a building stone, which represents one of the major causes of decay in the built environment.

In the case of *St. Margarethen*, the frost-thaw induced star cracks in as few as 14 cycles (see **Figure S3**). However, it should be noted that the test consists in accelerate aging, accentuating the real exposure conditions and cycling rate. The observed decay phenomena cannot be found on-site in the same manner. We explain this behavior by the testing conditions, which exaggerate the water content in the stone during freezing and thawing and cause a premature failing of the specimens [3]. Moreover, to provide an in-depth analysis, more cycles would be necessary to account for the microstructural decay of the fabric [4]. Nevertheless, the results suggest a certain susceptibility towards intrinsic mechanical processes.

No significant changes in apparent volume can be observed within the tested specimens although other methods show more significant alterations. The comparative measurements of ultrasound velocity and Young's modulus before and after the artificial aging, show measurable changes for *St. Margarethen*. It can be concluded that there is a significant difference in deterioration phenomena caused by frost and thawing for this lithotype, also indicated through the three out of six samples that could be analyzed.

Table S8. Overview of stone decay patterns found on-site, on the studied architectural element. The damage analysis was done by means of visual inspection and sample extraction for scanning electron microscopy (coupled with energy dispersive X-Ray spectroscopy) and optical microscopy. Three samples of different size have been extracted and investigated in form of stone chips, thin section, and polished cross section in the frame of the condition assessment analysis.

St. Margarethen calcareous fossil arenite – biosparite grain stone				
	Predominant decay phenomena		**Secondary decay phenomena**	
Decay pattern	**Sulphation (gypsum crust formation)**	**Sulphation**	**Granular disintegration**	**Erosion**
Key origin of microstructural defect	Mineral replacement reaction and pollutants incorporation	Mineral replacement reaction	Loss of microsparitic calcite binder, dissolution.	Selective loss of components due to chemical weathering (i.e., dissolution).
Depth of defect	On the surface of the rain-shadow areas	Up to 4 cm evidenced	Up to 2.5 cm in depth	Surface and subsurface zone
Width/thickness of defects	~5 mm thickness of black crust.	---	100 µm need to be bridged	---
Conservation requirements	Mechanical removal (e.g. micro chisels) and steam cleaning.	**Pre-consolidation** after chemically converting gypsum.	**Consolidation:** structural. **Protection:** coating can be considered.	**Consolidation:** structural. **Protection:** coating can be considered.

The predominant decay phenomenon is the calcite to gypsum transformation in varying depths and densities as well as the creation of black crusts on the surfaces of the studied lithotype. Secondary decay patterns observed on-site include granular disintegration and erosion. The consolidation focused on the former to restore the lost cohesion between the grains. Granular disintegration caused a weakened stone substrate and in severe cases, overlapping with additional decay patterns, a scaling and delamination. The granular disintegration was observed in form of micro cracks and a loss of the microsparitic calcite binder by means of microscopic techniques (see **Figures S4** to **Figure S8**). Furthermore, it was confirmed by means of drilling resistance measurements that the substrates soundness and mechanical strength were reduced (see **Figure S9**).

Beside these above-mentioned main decay phenomena, many other typical deterioration patterns have been documented according to the Icomos glossary on stone deterioration patterns [5]. The observed decay patterns included different types of biological colonization on the stone surfaces (e.g. moos, liches, fungus, algae, etc.), leaking joints, efflorescence, macroscopic cracks, the loss of stone substance and many more. It should be noted that an extensive restoration and conservation campaign including chemical and mechanical cleaning of black crusts and biological colonization was undertaken but is not presented in the frame of this work. Instead, the present work focused solely on the granular disintegration decay patterns that needed to be consolidated.

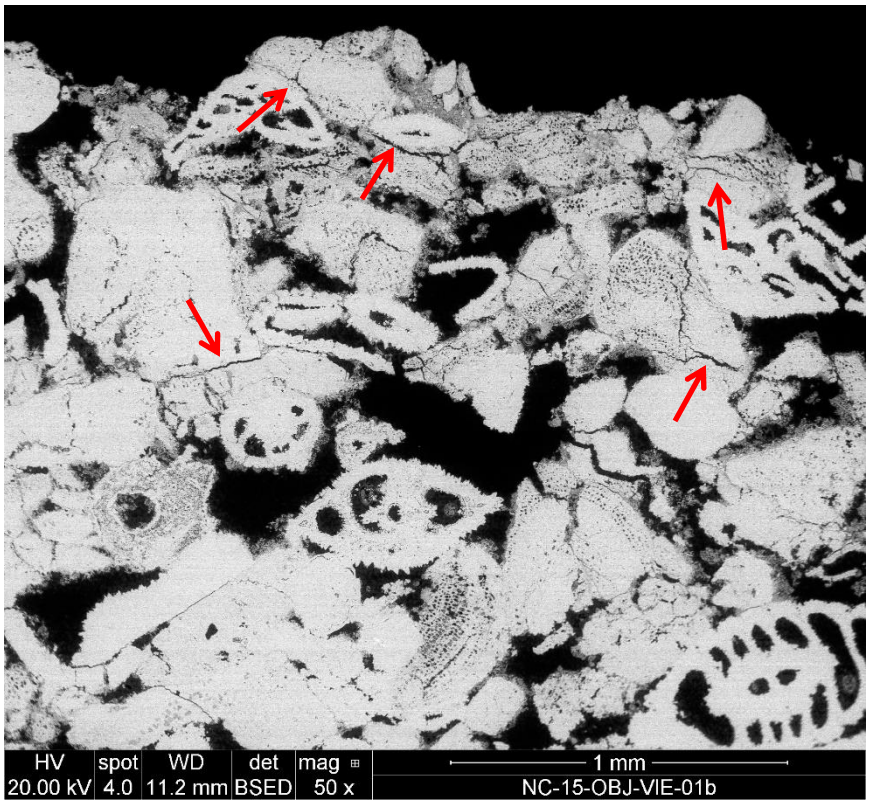

Figure S4. SEM-BSE, overview of the surface and subsurface zone exhibiting cracks parallel to the surface and between the fragments.

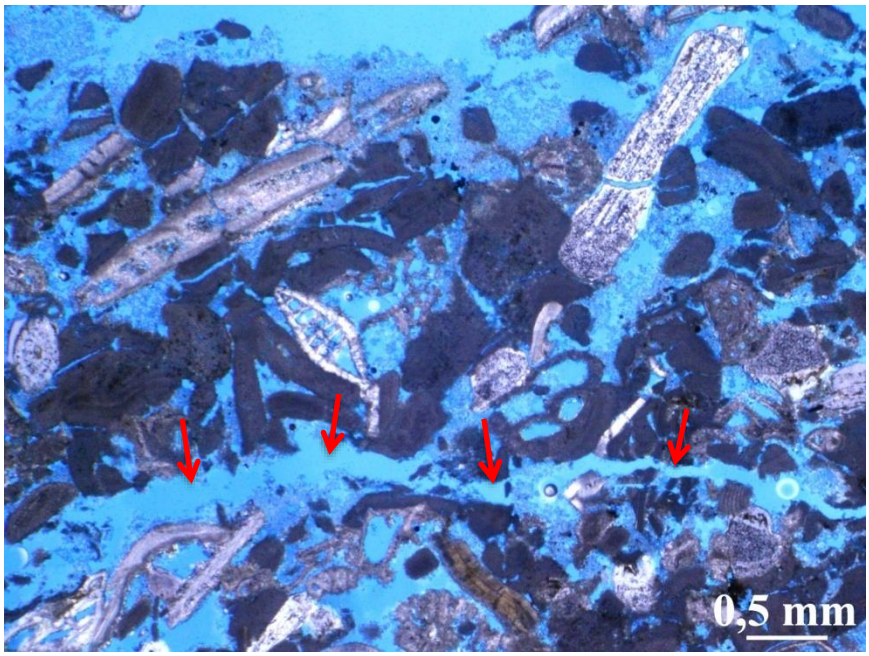

Figure S5. PLM micrograph, thin section, //N. View of a larger crack parallel to the surface.

Figure S6. SEM-BSE, stitched micrograph, overview of dissolution effects (upper part of the sample), granular disintegration with inter- and intragranular micro cracks and the porous microstructure.

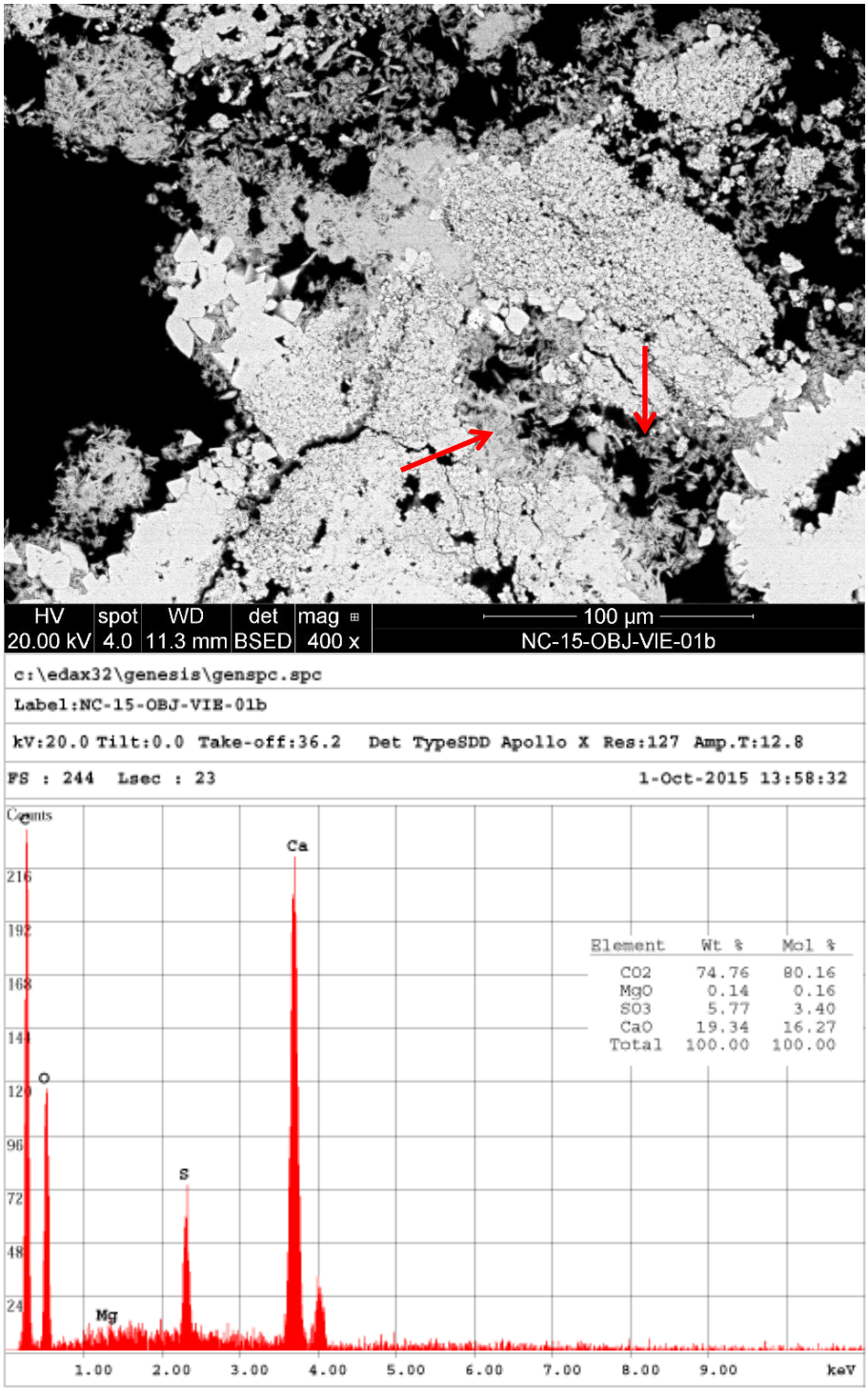

Figure S7. Upper figure: SEM-BSE, details of cracks and presence of gypsum (arrow-indicated). Lower graph: SEM-EDX analysis of the gypsum.

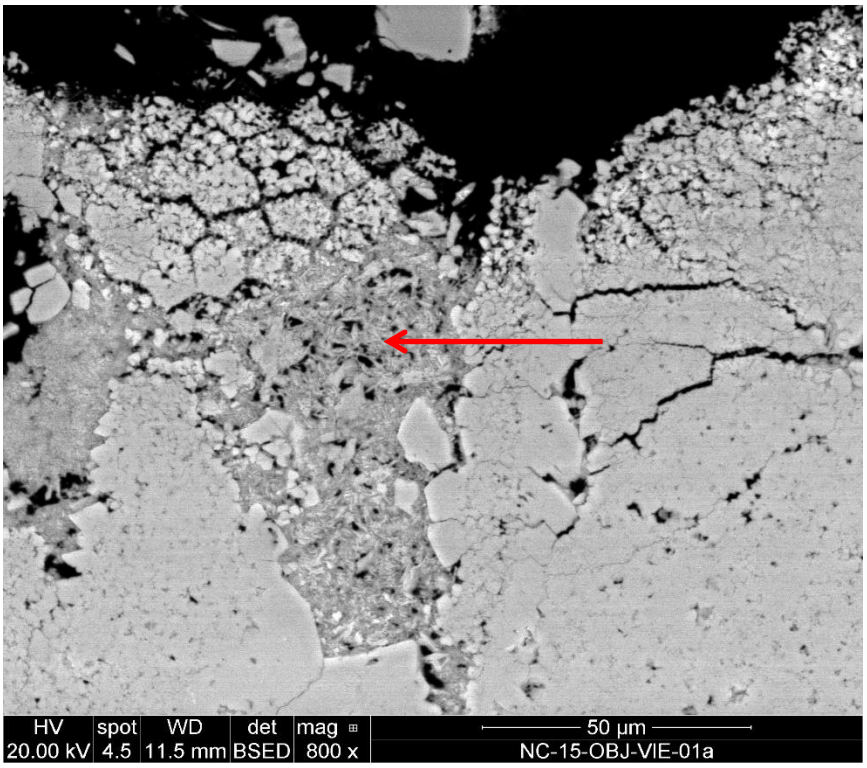

Figure S8. SEM-BSE, details of intragranular micro cracks and gypsum needles within the pores (arrow-indicated)

One of the main disadvantages of the studied on-site area was its variable morphology and thus varying porosity, as can be observed in **Table. S9**, **Figures S10** and **Figure S11**.

Table S9. Comparison of water absorption tests on-site to determine the condition of the substrate. An average of four tests was performed with the *Contact Sponge* method, with a contact time of 90 s. In addition, three tests have been performed with *Karsten Tube* and nine tests with the *Mirowski Pipe* to determine the water absorption coefficient after one hour.

Contact time	***Contact Sponge***	***Karsten Tube***	***Mirowski Pipe***
90 s [g m^{-2} s^{-1}]	6±4	197±187	12±6
60 min [kg m^{-2} $h^{-0.5}$]	---	23±12	31±18

These water absorption tests are commonly used to assess the condition of architectural surfaces [6]. The results reveal how inhomogeneous the substrate is, even when it seems homogeneous by visual inspection. Moreover, the wide spread of values in the initial stage of adsorption (i.e, Contact Sponge) as well as after one hour (i.e, Karsten Tube and Mirowski Pipe) indicates that an averaging is not possible. Furthermore, not only the surface but also the profile of degradation exhibits a substrate which condition is in need of a consolidation treatment (see **Figure S9**).

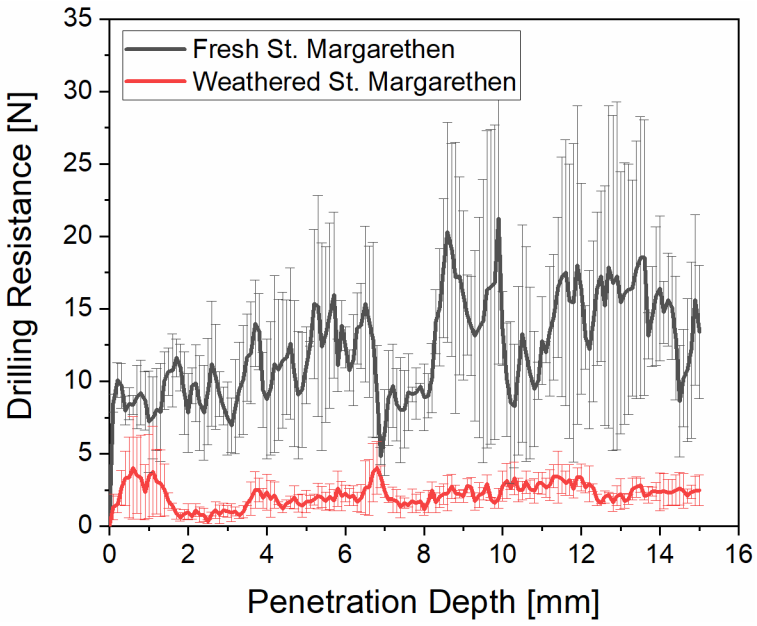

Figure S9. Drilling resistance measurement of weathered and fresh quarried *St. Margarethen*. The curve represents an average of three drilling holes for each condition. The weathered surfaces belong to the studied on-site areas where the consolidants were applied.

F**igure S10.** Intermediate restoration state, during the cleaning procedure and before treatment application. The rain exposed surfaces marked in red (top figure) have been used for consolidation purposes in the frame of this work. Bottom figures exhibit the differences in densities and decay patterns.

Figure S11. Intermediate restoration state, during the cleaning procedure and treatment application. The consolidants were applied by means of run-off methods with varying utensils.

Table S10. Effect of artificial ageing in respect to water absorption and ultrasound pulse velocity. The reported values were determined on six samples (5 x 5 x 5 cm) heat-treated from 500 °C to 600 °C.

Lithotype	Capillary absorption coefficient Initial value [kg/(m²h^0.5)] Increase ΔWAC [%]			Ultrasound pulse velocity Initial value [km/s] Decrease ΔUPV [%]		
	Mean	Min	Max	Mean	Min	Max
St. Margarethen	7.98 +12.07	6.03 +5.27	8.98 +27.56	3.57 –55.06	3.36 –43.41	3.87 –65.93

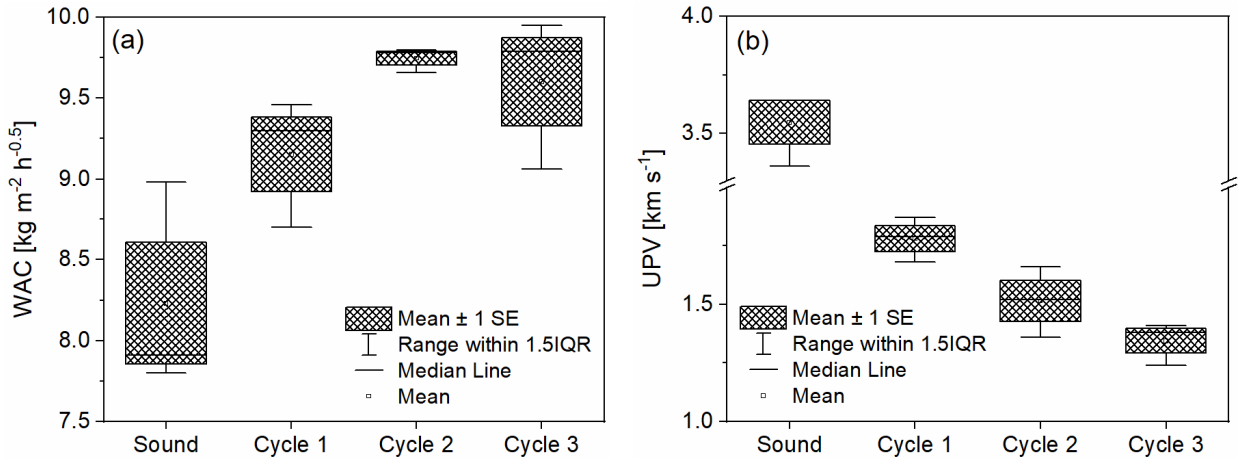

Figure S12. (a) Increase of water absorption coefficient [kg/(m²h^0.5)] and **(b)** decrease of ultrasound pulse velocity (km/s) after each cycle of heat treatment at 600 °C. An average of three specimens, 5 x 5 x 5 cm in size, is reported.

The predominate methods for checking the efficacy of the artificial ageing was ultrasonic pulse velocity (apparatus Labek, oscillation frequency 40 kHz) and water absorption coefficient after one hour. One concrete, reproducible result that could be attained quickly with thermal aging was a reduction in ultrasound pulse velocity and an increase of water absorption capillarity, both of which correspond to a reduction in a stone sample's soundness by formation of new micro cracks and the opening of existing cracks (see **Table S10** and **Figure S12**). A general finding of this pre-screening was that heating the stone is by far the most time efficient way to deteriorate and to reach a reduction of soundness reflective of the degradation processes observed in-situ (compare **Figure S4** to **Figure S8** with **Figure S13**), that is, the formation of micro cracks.

The degree of degradation is of major importance when studying stone consolidants; thus, a systematic approach to age the substrate is required. Moreover, the decay level can be specifically tailored, and a systematic investigation of the efficacy is possible. Therefore, the large-scale production of samples on which to test consolidants was mainly achieved through thermal treatment. Nevertheless, it should be noted that the results may vary drastically if specimens with different size are subjected to the same conditions of thermal aging.

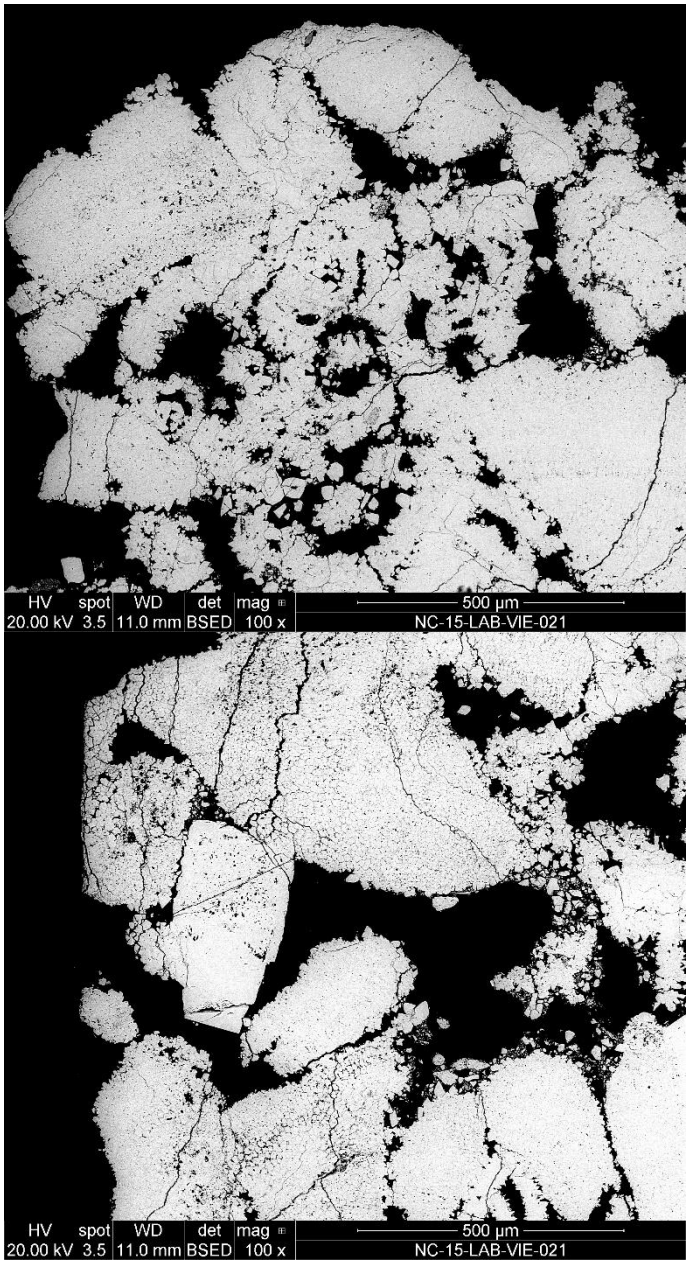

Figure S13. SEM-BSE, overview of artificially induced micro cracks by means of heat-treatment.

The artificially aged or heat-treated specimens allowed an inducement of micro cracks that can also be found on-site. However, their quantity and extent are not equivalent. The artificially aged specimens exhibit a more severe decay pattern when compared to the naturally weathered samples. Anyhow, the type, that is, the intergranular and intragranular micro cracks, can be observed on both, naturally and artificially aged specimens.

Table S11. Amount of consolidant applied on the test areas on-site. Two application cycles were performed by run-off, with an intermitted pause of 24 hours in between the cycles.

Consolidant	Area [cm^2]	1st cycle [ml]	[$ml \cdot cm^{-2}$]	2nd cycle [ml]	[$ml \cdot cm^{-2}$]	Total [$L \cdot m^{-2}$]
NC-25C (HFES70)	400	80	0.200	75	0.187	387
NC-12C (ZG12)	400	90	0.225	70	0.175	400
NC-29C (ZR110)	187	30	0.160	100	0.535	695

Note that the second application cycle of the treatment NC-29C (ZR110) tripled in comparison to the first cycle. It was observed that the consolidant did not equally penetrate the test area, some regions were adsorbing more while others stayed dump during the entire application procedure. We explain this behavior by either an intrinsic property of the lithotype (e.g. big inclusions of shell fragments) or a different aging pattern (e.g. varying degrees of mineral replacement reaction and thus formation of gypsum) causing distinct porosities.

It is important to note that the volume of the architectural element is large when compared to the chosen test areas. Therefore, we cannot make confident statements of where the consolidant was distributed. In other words, the actual penetration depth is not known as the consolidants might penetrate in the depths of the architectural element or they might also be distributed along the subsurface zones, or a combination of both.

Table S12. Amount of consolidant applied in laboratory on artificially aged (i.e., heat-treated) specimens with a size of 5 x 5 x 5 cm. The values represent an average calculated on 10 specimens per consolidant. Two application cycles were performed by capillary absorption for one hour, with an intermitted pause of 24 hours in between the cycles.

Consolidant	Area [cm^2]	1st cycle [ml]	[$ml \cdot cm^{-2}$]	2nd cycle [ml]	[$ml \cdot cm^{-2}$]	Total [$L \cdot m^{-2}$]
NC-25C (HFES70)	25	13.0 ±5.4	0.521	3.5 ±1.3	0.140	661
NC-12C (ZG12)	25	18.3 ±3.5	0.732	2.8 ±0.3	0.110	842
NC-29C (ZR110)	25	18.9 ±3.1	0.755	1.8 ±0.4	0.072	828

The absorbed amount changes with size and volume of the specimens as well as the conservation state of the substrate. It should be emphasized that a comparison between treatment applications performed in laboratory and on-site are not reliable. Effects like gravity, different treatment application (i.e., run-off and capillary absorption) and curing conditions (e.g. differing relative humidity, micro- and macroclimatic conditions, etc.) affect the outcome of the treatments performance and can therefore not be compared. It is particularly difficult to give meaningful specifications in the case of highly porous architectural elements, where the penetration depths and paths are unknown. In the case of laboratory treatment, for purposes of testing stone consolidants, capillary absorption is a preferred application method [7], as it assures a reproducible

way to apply a consolidant, making the interpretation of results easier. The total absorbed amount can therefore be described reliably only on laboratory treated specimens. In fact, not the total absorbed amount but the solid content after curing, is the governing factor and a direct function of the effectiveness of the consolidant [8]. As the solid content decreases in the following order NC-25C > NC-12C > NC-29C, it is easily accepted that the mechanical strength gain will follow the same trend, as can be confirmed by splitting tensile strength (performed in the laboratory) and drilling resistance measurements (performed on-site), see here for **Table S13**.

Table S13. Splitting tensile strength performed on laboratory specimens and average values (from 2 to 13 mm) of drilling resistance measurements performed on-site, before and after treatment application.

Test	**NC-25C**		**NC-12C**		**NC-29C**	
	Before	After	Before	After	Before	After
Splitting Tensile	1.13±0.1	2.13±0.2	1.13±0.1	1.52±0.2	1.13±0.1	1.42±0.3
Drilling Resistance	2.29±1	8.67±1.4	1.96±1	3.53±1.5	1.98±1.2	4.95±1.5

Note that the average values of drilling resistance measurements for the treatments NC-12C and NC-29C are not following the same trend regarding the above-mentioned solid content after curing when considering the mechanical strength gain. This deviation might be explained through the higher amount of consolidant applied on-site (see **Table S11**).

Table S14. Measures of variability for splitting tensile strength data.

Measures of Variability	Sound σ_t [N/mm^2]	Aged σ_t [N/mm^2]	NC-25C σ_t [N/mm^2]	NC-12C σ_t [N/mm^2]	NC-29C σ_t [N/mm^2]
Average	3.27	1.13	2.13	1.52	1.42
Standard deviation	0.41	0.14	0.19	0.24	0.34
Median	3.19	1.14	2.12	1.51	1.41
Minimum	2.79	0.88	1.89	1.23	0.89
Maximum	4.02	1.38	2.48	1.94	1.79

Table S14 reports on the measures of spread for the destructive test determining splitting tensile strength, as it is not possible to analyse a treatments performance on the same specimens before and after consolidation. Please note that the artificially aged specimens have been consolidated.

Acknowledgements
Lukas Achleitner, Anthony Baragona, Mario Blazevic, Anja Ziniel, Verena Hammerschmidt, Georg Heidfogel, Sofia Zamfirescu, Martin Pliessnig and Malkorzata Mozdyniewicz are gratefully acknowledged for their support in the lab and on-site. Johannes Weber and Andreas Rohatsch are recognised for their help in discussing the data and generally supporting this work.

Author Contributions
M.B. was the main responsible for the condition assessment on-site. E.M. performed the microscopy analysis. M.B. and E.M. evaluated and analysed the data jointly.

Reference
1. Moshammer B, Uhlir C, Rohatsch A, Unterwurzacher M (2015) Adnet 'Marble', Untersberg 'Marble'and Leitha Limestone—Best Examples Expressing Austria's Physical Cultural Heritage. Engineering Geology for Society and Territory Volume 5:253-257
2. Rohatsch A (2005) Neogene Bau-und Dekorgesteine Niederösterreichs und des Burgenlandes. In: Schwaighofer, B., Eppensteiner,W. (Eds.), "Junge" Kalke, Sandsteine und Konglomerate — Neogen. Mitteilungen IAG BOKU, pp. 27-31.,
3. Deprez M, De Kock T, De Schutter G, Cnudde V (2020) A review on freeze-thaw action and weathering of rocks. Earth-Science Reviews 203. doi:10.1016/j.earscirev.2020.103143
4. Ruedrich J, Kirchner D, Siegesmund S (2011) Physical weathering of building stones induced by freeze-thaw action: a laboratory long-term study. Environ Earth Sci 63 (7-8):1573-1586. doi:10.1007/s12665-010-0826-6
5. Verges-Belmin V (2008) Illustrated glossary on stone deterioration patterns. ICOMOS-ISCS (International Scientific Committee for Stone),
6. Vandevoorde D, Cnudde V, Dewanckele J, Brabant L, de Bouw M, Meynen V, Verhaeven E (2013) Validation of in situ applicable measuring techniques for analysis of the water adsorption by stone. Procedia Chem 8:317-327. doi:10.1016/j.proche.2013.03.039
7. Ferreira Pinto AP, Delgado Rodrigues J (2012) Consolidation of carbonate stones: Influence of treatment procedures on the strengthening action of consolidants. Journal of Cultural Heritage 13 (2):154-166
8. Ferreira Pinto A, Delgado Rodrigues J (2008) Stone consolidation: The role of treatment procedures. Journal of Cultural Heritage 9 (1):38-53. doi:10.1016/j.culher.2007.06.004